

Defect-free InAs nanowires self-catalyzed growth on graphene/Ge by molecular beam epitaxy

Yanhui Zhang(张燕辉), Haitao Jiang(姜海涛), Liuyan Fan(范柳燕), Zifan Huo(霍子帆), Ziteng Zhang(张孜腾), Can Zhou(周灿), Yajie Wang(王亚杰), Changlin Zheng(郑长林), Haibo Shu(舒海波), Xiaohao Zhou(周孝好), Pingping Chen(陈平平), Jin Zou(邹进), and Wei Lu(陆卫)

Citation: Chin. Phys. B, 2026, 35 (**3**): 038101. DOI: 10.1088/1674-1056/ae2bf3
http://cpb.iphy.ac.cn; http://iopscience.iop.org/cpb

What follows is a list of articles you may be interested in

High-temperature continuous-wave operation of 1310 nm InAs/GaAs quantum dot lasers

Xiang-Bin Su(苏向斌), Fu-Hui Shao(邵福会), Hui-Ming Hao(郝慧明), Han-Qing Liu(刘汗青),Shu-Lun Li(李叔伦), De-Yan Dai(戴德炎), Xiang-Jun Shang(尚向军), Tian-Fang Wang(王天放),Yu Zhang(张宇), Cheng-Ao Yang(杨成奥), Ying-Qiang Xu(徐应强), Hai-Qiao Ni(倪海桥),Ying Ding(丁颖), and Zhi-Chuan Niu(牛智川)

Chin. Phys. B, 2023, 32 (**9**): 098103. DOI: 10.1088/1674-1056/acb491

Plasma assisted molecular beam epitaxial growth of GaN with low growth rates and their properties

Zhen-Hua Li(李振华), Peng-Fei Shao(邵鹏飞), Gen-Jun Shi(施根俊), Yao-Zheng Wu(吴耀政), Zheng-Peng Wang(汪正鹏), Si-Qi Li(李思琦), Dong-Qi Zhang(张东祺), Tao Tao(陶涛), Qing-Jun Xu(徐庆君), Zi-Li Xie(谢自力), Jian-Dong Ye(叶建东), Dun-Jun Chen(陈敦军), Bin Liu(刘斌), Ke Wang(王科), You-Dou Zheng(郑有炓), and Rong Zhang(张荣)

Chin. Phys. B, 2022, 31 (**1**): 018102. DOI: 10.1088/1674-1056/ac339d

Vertical MBE growth of Si fins on sub-10 nm patterned substrate for high-performance FinFET technology

Shuang Sun(孙爽), Jian-Huan Wang(王建桓), Bao-Tong Zhang(张宝通), Xiao-Kang Li(李小康), Qi-Feng Cai(蔡其峰), Xia An(安霞), Xiao-Yan Xu(许晓燕), Jian-Jun Zhang(张建军), and Ming Li(黎明)

Chin. Phys. B, 2021, 30 (**7**): 078104. DOI: 10.1088/1674-1056/abf63f

Growth of high-crystallinity uniform GaAs nanowire arrays by molecular beam epitaxy

Yu-Bin Kang(亢玉彬), Feng-Yuan Lin(林逢源), Ke-Xue Li(李科学), Ji-Long Tang(唐吉龙), Xiao-Bing Hou(侯效兵), Deng-Kui Wang(王登魁), Xuan Fang(方铉), Dan Fang(房丹), Xin-Wei Wang(王新伟), and Zhi-Peng Wei(魏志鹏)

Chin. Phys. B, 2021, 30 (**7**): 078102. DOI: 10.1088/1674-1056/abf920

Epitaxial growth and air-stability of monolayer Cu_2Te

K Qian(钱凯), L Gao(高蕾), H Li(李航), S Zhang(张帅), J H Yan(严佳浩), C Liu(刘晨), J O Wang(王嘉鸥), T Qian(钱天), H Ding(丁洪), Y Y Zhang(张余洋), X Lin(林晓), S X Du(杜世萱), H-J Gao(高鸿钧)

Chin. Phys. B, 2020, 29 (**1**): 018104. DOI: 10.1088/1674-1056/ab5781

RAPID COMMUNICATION

Defect-free InAs nanowires self-catalyzed growth on graphene/Ge by molecular beam epitaxy

Yanhui Zhang(张燕辉)[1,4,†,‡], Haitao Jiang(姜海涛)[2,†], Liuyan Fan(范柳燕)[1], Zifan Huo(霍子帆)[1], Ziteng Zhang(张孜腾)[1], Can Zhou(周灿)[1], Yajie Wang(王亚杰)[3], Changlin Zheng(郑长林)[3], Haibo Shu(舒海波)[5,§], Xiaohao Zhou(周孝好)[1,4], Pingping Chen(陈平平)[1,4,¶], Jin Zou(邹进)[6,7], and Wei Lu(陆卫)[1,4,8]

[1] *State Key Laboratory of Infrared Physics, Shanghai Institute of Technical Physics, Chinese Academy of Sciences, Shanghai* 200083, *China*
[2] *State Key Laboratory of Materials for Integrated Circuits, Shanghai Institute of Microsystem and Information Technology, Chinese Academy of Sciences, Shanghai* 200050, *China*
[3] *State Key Laboratory of Surface Physics and Department of Physics, Fudan University, Shanghai* 200438, *China*
[4] *University of Chinese Academy of Sciences, Beijing* 100049, *China*
[5] *College of Optical and Electronic Technology, China Jiliang University, Hangzhou* 310018, *China*
[6] *Materials Engineering and Centre for Microscopy and Microanalysis, The University of Queensland, QLD* 4072, *Australia*
[7] *Institute of Energy Materials Science, University of Shanghai for Science and Technology, Shanghai* 200093, *China*
[8] *School of Physical Science and Technology, Shanghai Tech University, Shanghai* 201210, *China*

(Received 11 November 2025; revised manuscript received 12 December 2025; accepted manuscript online 12 December 2025)

InAs nanowires (NWs) self-catalyzed grown on graphene surface frequently exhibit a large number of stacking-fault defects. However, the control of these defects in InAs NWs still remains a large challenge, which significantly limits the applications of InAs NWs in electronics and optoelectronics. In this work, the self-catalyzed growth of InAs NWs on graphene/Ge substrate by molecular beam epitaxy (MBE) is systematically investigated. Growth models for InAs NWs and parasitic islands on graphene/Ge are developed. Through rational design of growth parameters, the self-catalyzed growth of defect-free InAs NWs on graphene surfaces is ultimately achieved. Our experimental results indicate that lower growth temperature can effectively suppress the formation of stacking-fault defects in InAs NWs, no visible stacking-fault defects are observed in the samples grown below 510 °C, and the intrinsic mechanism for this is clarified with the density functional theory (DFT) calculations.

Keywords: InAs nanowires (NWs), molecular beam epitaxy (MBE), self-catalyzed growth, density functional theory (DFT)

PACS: 81.15.Hi, 62.23.Hj, 68.65.–k

DOI: 10.1088/1674-1056/ae2bf3 **CSTR:** 32038.14.CPB.ae2bf3

III–V NWs exhibit huge potential for a wide range of applications in the fields of electronic, photonic, and optoelectronic devices.[1–3] In recent studies, the substrates for growing III–V NWs were mainly rigid substrates such as GaAs and Si.[4–6] With the development of electronic devices towards flexibility, lightweight, and integration, the growth of transferable III–V NWs on 2D materials such as graphene surface received more attention.[7–17] The hexagonal symmetric structure of graphene is suitable as a substrate for vertically grown cubic or hexagonal semiconductor NWs,[10] and graphene also has many properties such as conductivity, thermal conductivity, transparency, flexibility, and no dangling bonds on the surface (facilitate the detachment of epitaxial materials from graphene). Therefore, the fabrication of mixed-dimensional NW/graphene heterojunctions is highly promising for the development of flexible NW optoelectronic devices and multi-functional NW heterojunction integrated devices.[18,19]

InAs NWs have the characteristics such as narrow bandgap, high mobility, and easy formation of Ohmic contacts, which are useful for infrared photodetectors, high-frequency electronic devices, and spin devices.[20–22] So far, many studies have achieved catalyst-free and self-catalyzed growth of InAs NWs on various graphene substrates such as graphite, mechanically exfoliated multilayer graphene, and chemical vapor deposition (CVD) graphene grown on metal substrates.[23–27] In these studies, the commonly used mechanically exfoliated graphite flakes and graphene transferred from metal substrates generally do not possess the characteristics of ideal substrates such as high quality, cleanliness, and large-area uniformity, and are not suitable for growing samples for large-scale applications. In addition, the growth process of InAs NWs on the surface of graphene, especially for their

[†] These authors contributed equally to this work.
[‡] Corresponding author. E-mail: zyhq@mail.sitp.ac.cn
[§] Corresponding author. E-mail: shuhaibo@cjlu.edu.cn
[¶] Corresponding author. E-mail: ppchen@mail.sitp.ac.cn

© 2026 Chinese Physical Society and IOP Publishing Ltd. All rights, including for text and data mining, AI training, and similar technologies, are reserved.

nucleation and defect formation mechanism, is not clear and requires in-depth understanding. Although the self-catalyzed growth of InAs NWs on graphene surface avoids the foreign metal catalyzers suspected to being incorporated during NW growth, the grown InAs NWs still suffer from high densities of stacking faults.[23–27]

In this study, graphene/Ge substrates with larger area and high quality were first prepared by CVD method,[28,29] then defect-free InAs NWs were successfully synthesized on graphene/Ge by MBE. Growth process and key influencing factors of the InAs NWs on graphene/Ge were investigated systematically, and the nucleation and growth model of InAs NWs and parasitic islands on graphene/Ge surfaces was provided. In addition, we studied the effects of growth temperature on the stacking faults in InAs NWs and investigated its intrinsic mechanism through DFT calculation.

Figure 1(a) shows a schematic diagram of the growth process of InAs NWs on graphene/Ge substrate. Firstly, graphene/Ge substrate is prepared by CVD, and typical atomic force microscope (AFM) image and Raman spectrum of the graphene/Ge are shown in Fig. S1. At the beginning of InAs NWs growth, In droplets are formed on graphene surface, and then nucleation and growth of InAs NWs are realized initiated through the In droplets. Hence, the growth in the initial stage of InAs NWs should belong to vapor-liquid-solid (VLS) mode. With the growth under an As rich environment, In droplets are gradually consumed and switch to vapor-solid (VS) growth mode. Figure 1(b) shows a SEM image of InAs NWs grown on graphene/Ge (100), in which vertically grown InAs NWs with a length of over 3.5 μm and a diameter between 80–120 nm on graphene/Ge can be seen. No catalyst particles can be found at the top of InAs NWs, similar to most reported InAs NWs grown on graphene surfaces.[23–27] Interestingly, no InAs NWs were directly grown on Ge (100), Ge (110) and Ge (111) substrates, but self-catalyzed InAs NWs can be grown on graphene covered Ge (100), Ge (110) and Ge (111) substrates (Figs. S2–S4). These results indicate that graphene plays a critical role in growing vertical InAs NWs, while the impact of Ge substrate is not significant.

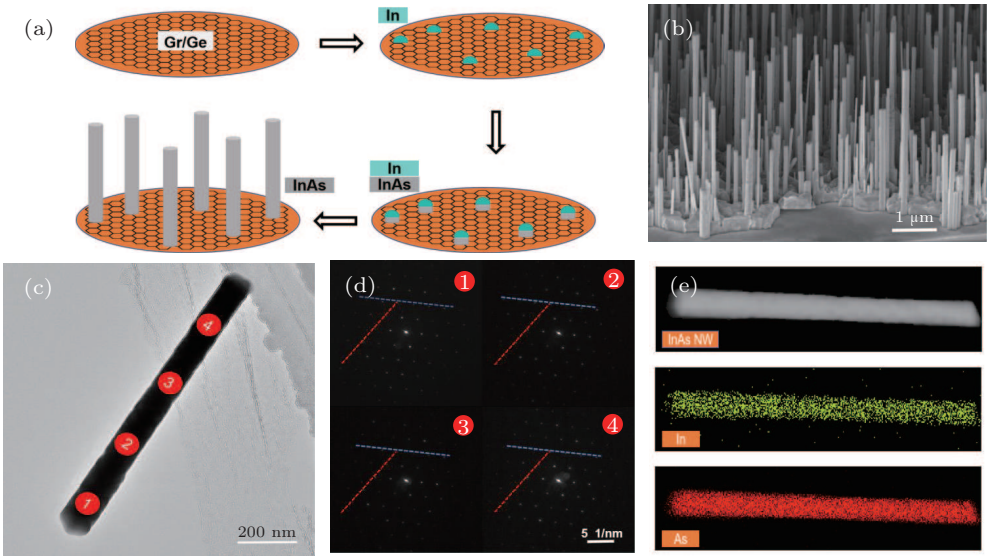


Fig. 1. InAs NWs grown on graphene/Ge. (a) Schematic diagram of vertical InAs NWs grown on graphene/Ge. (b) 70° tilted-view SEM images of InAs NWs grown on graphene/Ge (100). (c) Low-magnification TEM image of an InAs NW. (d) SAED patterns recorded from different regions (1–4) of the nanowire shown in panel (c). (e) Low-magnification STEM image and corresponding EDX elemental mapping of In and As for the nanowire shown in panel (c).

To examine the crystal structure and elemental composition uniformity of the NWs, we conducted electron microscopic investigations using a field-emission transmission electron microscope (TEM, Talos F200i, Thermo Fisher Scientific). Figure 1(c) shows an overview TEM image of a single InAs nanowire, with four numbered regions selected for subsequent electron diffraction analysis. The corresponding selected area electron diffraction (SAED) patterns, which are shown in Fig. 1(d), reveal that the nanowire has a zinc blende (ZB) phase. The alignment of all four SAED patterns along the NWs length indicates a uniform crystal structure and orientation throughout. Figure 1(e) shows the elemental mapping of the same NW (Fig. 1(c)) using energy-dispersive x-ray spectroscopy (EDX) in scanning transmission electron microscopy (STEM) mode. The composition ratio of In to As is approximately 1:1, uniformly distributed across the entire NW. Detailed measurement data can be found in Fig. S5.

To clarify the nucleation and growth process of InAs NWs on graphene/Ge, the morphology as well as the interface between InAs and graphene substrate were studied in detail. Figure 2(a) shows a typical SEM top view image of InAs on graphene/Ge, the epitaxial InAs can be roughly divided into two categories: hexagonal InAs nanowire (marked with 1), shapeless parasitic island (marked with 2). Figure 2(b) shows

an overview cross-sectional TEM image of an InAs NW and the graphene substrate, with three marked regions corresponding to the InAs nanowire, the interface and the Ge substrate. The corresponding fast Fourier transform (FFT) from atomic resolution images of these regions is shown in Figs. 2(f)–2(h). Discrete dots in Figs. 2(f) and 2(h) demonstrate that both the InAs nanowire and the Ge substrate are high-quality single crystals. Note that the FFT pattern of single-layer graphene is not visible due to the limited size. The FFT pattern in Fig. 2(g) is a superposition of the two sets of individual diffraction patterns in Figs. 2(f) and 2(h), indicating that the interface between InAs nanowire and the graphene/Ge substrate is sharp and does not form a thick polycrystalline buffer layer. Figure 2(c) shows a high-resolution TEM image of the InAs nanowire and graphene/Ge substrate interface region. This image reveals atomically sharp interfaces (shown by dashed lines), except for a lattice distortion of only two atomic layers in the dashed box region. This region could be the nucleation point of the InAs nanowire, possibly introduced by a small defect in the graphene. From Fig. 2(c), it can be seen that the range of lattice distortion is only two atomic layers in the vertical direction and less than 5 nm in the horizontal direction. Therefore, due to the weak van der Waals interaction between nanowires and graphene in the normal region, the stress generated by lattice distortion in the nucleation region is released laterally and does not extend longitudinally.

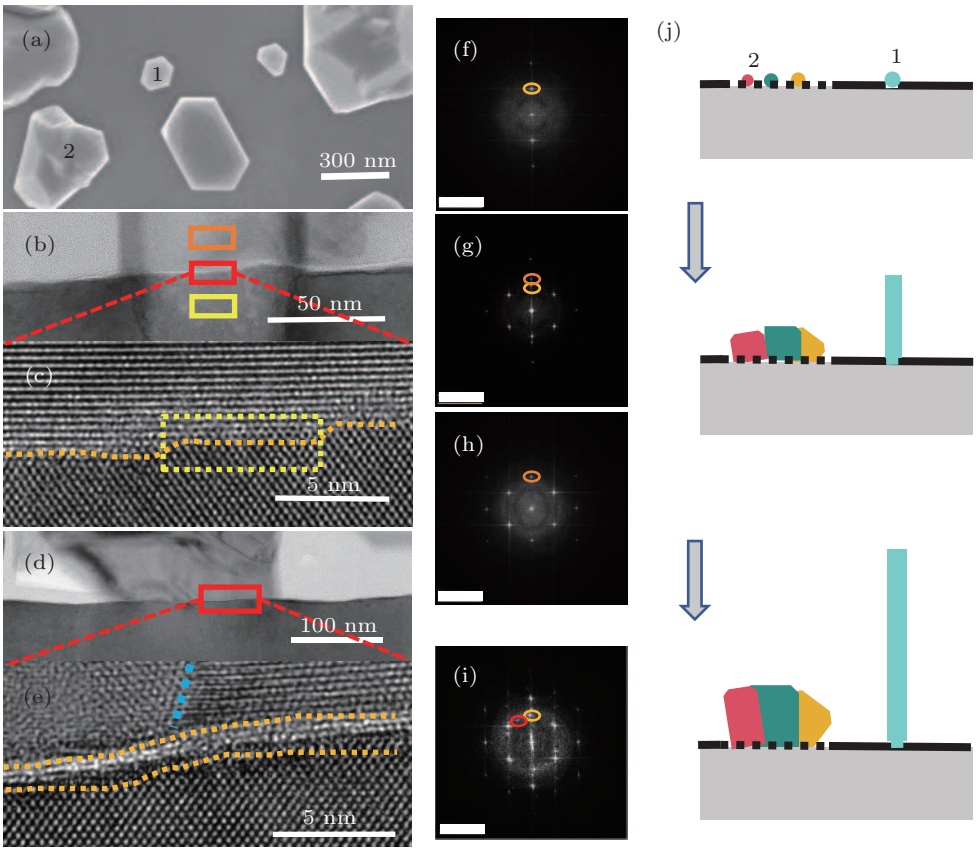


Fig. 2. Heteroepitaxy model of InAs on graphene/Ge. (a) SEM image of InAs NWs taken at top view. (b) Cross-sectional TEM image of an InAs nanowire grown on graphene/Ge. (c) High-resolution TEM image of the enclosed area in panel (b). (f)–(h) FFT of the InAs nanowire (top panel), the interface of InAs and graphene/Ge (middle panel), and the Ge substrate (bottom panel) in panel (b). (d) Cross-sectional TEM image of an InAs parasitic island grown on graphene/Ge. (e) High-resolution TEM image and (i) FFT of the InAs parasitic island of the enclosed area in panel (d). (j) The growth model for the InAs nanowire and parasitic island on graphene/Ge.

Figure 2(d) shows a low-magnification TEM image of the interface between an InAs parasitic island and graphene/Ge substrate. The region marked with a panel is magnified in Fig. 2(e), with its corresponding FFT pattern shown in Fig. 2(i). Comparing Figs. 2(g) and 2(i) reveals an extra set of diffraction patterns (highlighted by a red circle). Figure 2(e) also demonstrates different atomic structures on either side of the blue dashed line, both indicating that the parasitic island in that regions has two distinct crystal orientations. Unlike the sharp interface between the InAs nanowire and substrate (Fig. 2(c)), the interface between InAs parasitic island and substrate exhibits approximately 4–5 atomic layers of structural disorder. This suggests more defects in the graphene in this region.

Based on the results in Figs. 2(a)–2(i), an epitaxial model of InAs on graphene/Ge substrate is proposed, as shown in Fig. 2(j). In atoms deposited on the graphene surface will aggregate to form crystal nuclei at defect areas. At the small defect areas, the role of the small defects is only to promote nucleation, and the direction of nucleation is determined by

graphene, a single-crystal nucleus will form easily and grow along the ⟨111⟩ direction under the induction of graphene to form InAs NWs (marked with 1). In severely damaged areas, the edges of graphene and exposed Ge surface would induce multiple nuclei with different orientations. These nuclei grow and connect together, forming polycrystalline parasitic islands (marked with 2). In the InAs nanowire sample with a growth time of 2 min, there is significant lateral growth of the nanowire at the large-sized defects, which should be influenced by the Ge (100) crystal plane (Fig. S6), Therefore, big defects are not suitable for the nucleation of NWs. During the growth, the atoms for InAs (including NWs and parasitic islands) crystal nucleus growth mainly comes from atomic diffusion around the crystal nucleus, the amount of atoms that a crystal nucleus can obtain is related to its density and atomic migration ability. Assuming that the density of crystal nucleus is the same, the number of atoms obtained for each nucleus is also the same. Therefore, InAs NWs with smaller lateral dimensions are higher than parasitic islands.

TEM investigations, as shown in Fig. 3, further reveal the impact of growth temperature on the morphology and crystal structure of InAs NWs on graphene/Ge. Comparing Figs. 3(a)–3(c), it can be found that at lower growth temperature, the shape of the InAs NWs is less regular and the surface is rougher. By increasing the growth temperature, the thickness and surface roughness of InAs NWs tend to be uniform. The atomic resolution TEM images also show that the atomic structures of NWs change at different growth temperatures. Figure 3(e) shows that the InAs nanowire grown at 480 °C is pure ZB phase, while Fig. 3(f) shows pure WZ phase (at 510 °C). At the highest temperature of 570 °C, the nanowire contains mixed phase structure (Fig. 3(g)). More SAED results demonstrate that at lower growth temperature, both ZB and WZ phase InAs NWs can be found on the same graphene/Ge substrate, and have no stacking-fault defects. However, InAs NWs grown at higher temperature generally have obvious stacking-fault defects (Fig. S7). As shown in the atomic resolution high angle annular dark field STEM (HAADF-STEM) images, the NWs grown at higher temperature (above 540 °C) contain many stacking-fault defects (Fig. 3(d)), which lead to the appearance of mixing phase and twinning. In the lower growth temperature sample (below 510 °C, Fig. 3(h)), no defects are visible.

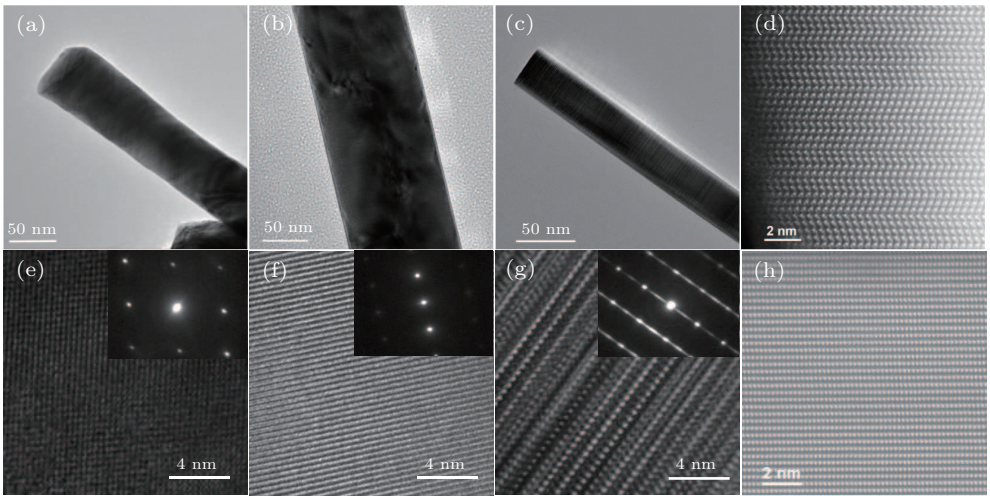


Fig. 3. Effect of growth temperature on the crystal structure of InAs NWs on graphene/Ge. (a)–(c) Low-magnification TEM images of InAs NWs grown at 480 °C, 510 °C, and 570 °C transferred to copper mesh. (e)–(g) The corresponding atomic resolution TEM images (a)–(e), (b)–(f), (c)–(g) with SAED patterns inserted. Typical atomic resolution HAADF-STEM images of two kinds of InAs NWs at higher (d) and lower (h) growth temperatures.

The above results suggest that the growth temperature is an important factor for affecting the growth of InAs NWs on the graphene. More specifically, the lower growth temperature can effectively suppress the formation of stacking-fault defects in InAs NWs, but it simultaneously makes the grown InAs NWs become thick and short and present inconsistent diameters. The increase of the growth temperature can promote the axial growth, resulting in uniform InAs NWs. However, excessively high temperatures introduce stacking-fault defects into InAs NW lattice. Therefore, taking into account the length of InAs NWs and stacking-fault defects, the growth temperature should be set to the maximum value without forming stacking-fault defects. In addition, since the growth temperature is not the only parameter that affects growth, the specific growth temperature setting needs to comprehensively consider other parameters such as the flux ratio of In and As.

In order to insight into the temperature-dependent phase structure of InAs NWs, a nucleation model based on the self-catalytic nucleation theory is proposed (see the details in the supporting information). For the self-catalyzed growth of InAs NWs following a vapor-solid mechanism, the formation enthalpy (ΔG) for producing a nucleus on the top of the nanowire

(see Fig. 4(a)) can be calculated as follows:

$$\Delta G = -n\Delta\mu + B\gamma_{\rm vs} + A\gamma_{\rm sn}, \tag{1}$$

where $\Delta\mu$ is the change in chemical potential per In–As pair, n is the number of In–As pair in the formed nucleus, $\gamma_{\rm vs}$ is the surface energy of the side facet of the nucleus, $\gamma_{\rm sn}$ is the twin formation energy, A is the area of the upper or bottom surface of the nucleus, and B is surface area of side facets. All these surface energies and formation energies are determined by density-functional theory (DFT) calculations and listed in Table S1. When the formed nucleus is not a twin structure, $\gamma_{\rm sn}$ is equal to zero. The nucleation on InAs nanowire requires to overcome a nucleation barrier ΔG^* (i.e., the maximum of formation enthalpy). Accordingly, the formation enthalpy ΔG^* for the critical nucleus with a twin structure is given by

$$\Delta G_t^* = \Delta G(\rho_t^*) = -\frac{3\rho_t^{*2}}{a_0^2}\Delta\mu + \frac{3\sqrt{3}}{2}\rho_t^{*2}\gamma_{\rm sn} + \frac{6h\rho_t^*\gamma_{\rm vs}}{\cos\theta}. \tag{2}$$

When the formed nucleus lacks the twin structure, ΔG^* can be expressed as

$$\Delta G^* = \Delta G(\rho^*) = -\frac{3\rho^{*2}}{a_0^2}\Delta\mu + \frac{6h\rho^*\gamma_{\rm vs}}{\cos\theta}. \tag{3}$$

Based on the approach of Johansson *et al.*,[30] the nucleation of a facet x on pre-existing nanowire surface y is governed by an exponential distribution with probability

$$P(x|y) = \exp\left(-\frac{\Delta G_{xy}^*}{k_{\rm B}T}\right)/\sum_i \exp\left(-\frac{\Delta G_{iy}^*}{k_{\rm B}T}\right), \tag{4}$$

where i represents all possible orientations of nucleation facets, $k_{\rm B}$ is the Boltzmann constant, and T is the growth temperature (K). For the growth of pure ZB nanowire, it requires the probability for the formation of a twin structure is equal to zero, i.e., Pt $\to$ 0. For the growth of pure WZ nanowire, it requires Pt $\to$ 1. When Pt locates between 0.1 and 0.9, the stacking faults or twin defects will be formed in the nanowires. Here we considered the formed nucleus with different side facets. If the formed nucleus has a ZB phase, its side facets can be $\{1\bar{1}0\}$, $\{11\bar{1}\}A/\{11\bar{1}\}B$, and $\{001\}/\{00\bar{1}\}$. For the formed nucleus with a WZ phase, its side facets can be $\{1\bar{1}00\}$ and $\{11\bar{2}0\}$. Based on Eqs. (1)–(4), the nucleation barrier ΔG^* for the formed nucleus with various potential side facets as a function of $\Delta\mu$ is plotted in Fig. 4(b). It can be found that the ZB-phase nucleus with $\{11\bar{1}\}A$ and $\{11\bar{1}\}B$ side facets exhibits the lowest ΔG^* for $\Delta\mu < 0.25$ eV and the WZ-phase nucleus with $\{11\bar{2}0\}$ side facets has the lowest ΔG^* when $\Delta\mu$ is larger than 0.25 eV, implying that the formed nanowire structure prefers to the ZB phase under the lower $\Delta\mu$. The increase of $\Delta\mu$ could lead to the formation of twin structure with the WZ phase. In order to better understand the crystal phase

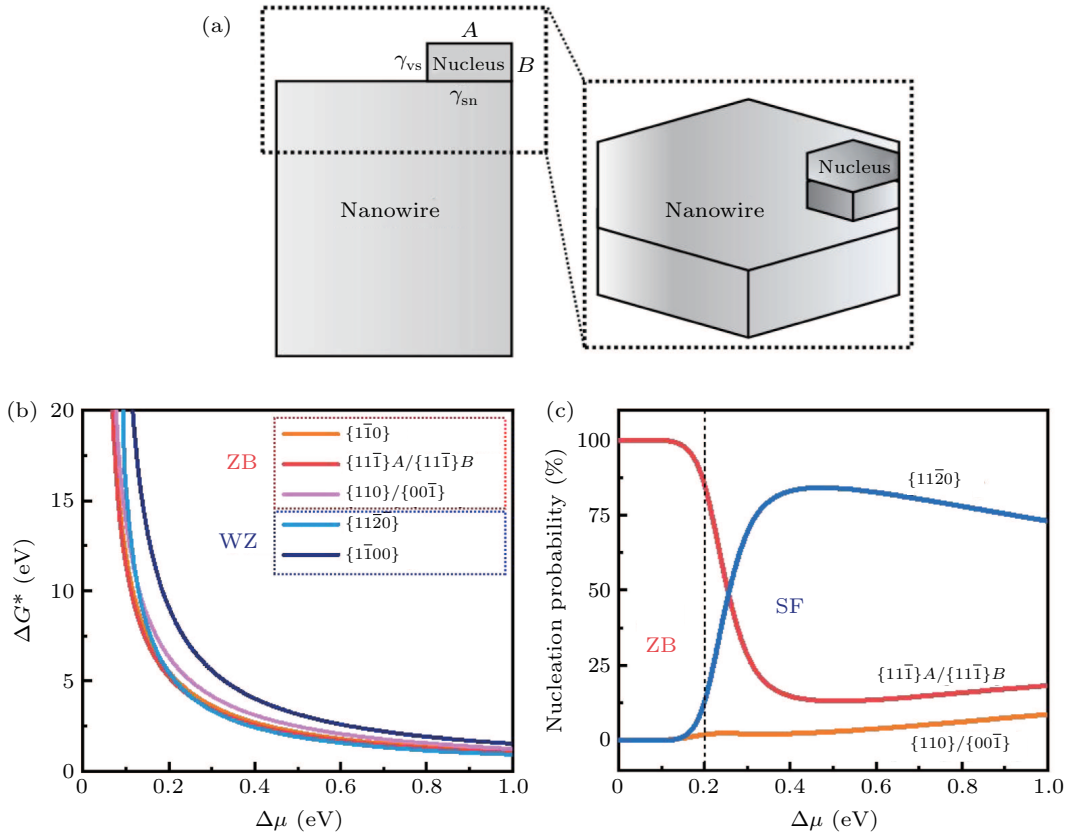


Fig. 4. Schematic illustrations of the nucleus and InAs nanowire. (b) Nucleation barrier ΔG^* and (c) nucleation probability P as a function of $\Delta\mu$ for the formation of a nucleus with different side facets during the growth of InAs nanowires.

of the formed nucleus during the growth of InAs NWs, the nucleation probability P as a function of $\Delta\mu$ is presented in Fig. 4(c). For the lower $\Delta\mu$ (e.g., $\Delta\mu < 0.2$ eV), the as-grown InAs nanowires will be dominated by the ZB phase. With the increase of $\Delta\mu$, the nucleation probability of WZ phase rapidly increases. This means that there exists a competition between WZ and ZB phases at higher $\Delta\mu$, consequently resulting in the mixed WZ and ZB phases (i.e., stacking faults) in the formed nanowires. The relationship between the $\Delta\mu$ and temperature T as well as the concentration of In and As flux can be described by

$$\Delta\mu = k_{\mathrm{B}}T \ln \frac{C_{\mathrm{In}}C_{\mathrm{As}}}{C_{\mathrm{In,eq}}C_{\mathrm{As,eq}}}, \tag{5}$$

where C_{In} and C_{As} denote the concentrations of In and As fluxes during the growth, and $C_{\mathrm{In,eq}}$ and $C_{\mathrm{As,eq}}$ denote the concentrations of In and As under the equilibrium condition, respectively. A high growth temperature induces a large $\Delta\mu$. Therefore, the increase of growth temperature can drive the structure of InAs NWs from the pure ZB phase to the mixed ZB and WZ phase (or stacking faults), which agrees well with our experimental observations.

In summary, the defect-free InAs NWs on graphene/Ge were successfully demonstrated by a self-catalytic growth strategy via the MBE method. The nucleation of InAs on graphene/Ge is sensitive to the defects in the graphene. The introduction of appropriate defects in graphene substrate could greatly promote the nucleation of InAs NWs, but larger defects could lead to the formation of parasitic islands. The higher growth temperature is beneficial for the growth of InAs NWs, but excessively high temperature readily leads to the formation of stacking-fault defects. The theoretical calculations show that there is a delicate competition between the WZ and ZB phases at the higher temperature, leading to the occurrence of mixed phases. This study enriches the heteroepitaxial theory on 2D substrates and promotes the application of nanowire arrays in flexible devices and heterojunction integration.

See the supplementary material for Figs. S1–S7 and details of theoretical calculations.

Acknowledgments

Project supported by the Robotic AI-Scientist Platform of Chinese Academy of Sciences, the National Natural Science Foundation of China (Grant Nos. 12027805, 62171136, and 12227901), and Programs of Shanghai Science and Technology Commission (Grant No. 22501100202).

References

[1] Takahashi T, Takei K, Adabi E, Fan Z, Niknejad A M and Javey A 2010 *ACS Nano* **4** 5855
[2] Han N, Wang F, Hou J J, Yip S P, Lin H, Xiu F, Fang M, Yang Z, Shi X and Dong G 2013 *Adv. Mater.* **25** 4445
[3] Gudiksen M S, Lauhon L J, Wang J, Smith D C and Lieber C M 2002 *Nature* **415** 617
[4] Pan D, Fu M, Yu X, Wang X, Zhu L, Nie S, Wang S, Chen Q, Xiong P and Von Molnár S 2014 *Nano Lett.* **14** 1214
[5] Zhang Z, Zheng K, Lu Z Y, Chen P P, Lu W and Zou J 2015 *Nano Lett.* **15** 876
[6] Kang J H, Cohen Y, Ronen Y, Heiblum M, Buczko R, Kacman P, Popovitz-Biro R and Shtrikman H 2013 *Nano Lett.* **13** 5190
[7] Tchoe Y, Jo J, Kim M and Yi G C 2015 *NPG Asia Mater.* **7** e206
[8] Hong Y J and Fukui T 2011 *ACS Nano* **5** 7576
[9] Nalamati S, Sharma M, Deshmukh P, Kronz J, Lavelle R, Snyder D, Reynolds Jr C L, Liu Y and Iyer S 2019 *ACS Appl. Nano Mater.* **2** 4528
[10] Munshi A M, Dheeraj D L, Fauske V T, Kim D C, van Helvoort A T, Fimland B O and Weman H 2012 *Nano Lett.* **12** 4570
[11] Tchoe Y, Jo J, Kim H, Kim H, Baek H, Lee K, Yoo D, Choi W J, Kim M and Yi G C 2021 *NPG Asia Mater.* **13** 33
[12] Fernández-Garrido S, Ramsteiner M, Gao G, Galves L A, Sharma B, Corfdir P, Calabrese G, de Souza Schiaber Z, Pfüller C and Trampert A 2017 *Nano Lett.* **17** 5213
[13] Wallentin J, Kriegner D, Stangl J and Borgström M T 2014 *Nano Lett.* **14** 1707
[14] Heilmann M, Munshi A M, Sarau G, Göbelt M, Tessarek C, Fauske V T, van Helvoort A T, Yang J, Latzel M and Hoffmann B r 2016 *Nano Lett.* **16** 3524
[15] Lee C H, Kim Y J, Hong Y J, Jeon S R, Bae S, Hong B H and Yi G C 2011 *Adv. Mater.* **23** 4614
[16] Jeong J, Wang Q, Cha J, Jin D K, Shin D H, Kwon S, Kang B K, Jang J H, Yang W S and Choi Y S 2020 *Sci. Adv.* **6** eaaz5180
[17] Ren D, Nilsen T A, Nilsen J S, Ahtapodov L, Mukherjee A, Li Y, van Helvoort A T, Weman H and Fimland B O 2024 *ACS Appl. Nano Mater.* **7** 6797
[18] Anyebe E A and Kesaria M 2021 *Nano Select* **2** 688
[19] Hong Y J, Saroj R K, Park W I and Yi G C 2021 *APL Mater.* **9** 060907
[20] Miao J, Hu W, Guo N, Lu Z, Zou X, Liao L, Shi S, Chen P, Fan Z, Ho J C, Li T X, Chen X S and Lu W 2014 *ACS Nano* **8** 3628
[21] Dayeh S A, Aplin D P, Zhou X, Yu P K, Yu E T and Wang D 2007 *Small* **3** 326
[22] Nadj-Perge S, Frolov S, Bakkers E and Kouwenhoven L P 2010 *Nature* **468** 1084
[23] Kang J H, Ronen Y, Cohen Y, Convertino D, Rossi A, Coletti C, Heun S, Sorba L, Kacman P and Shtrikman H 2016 *Semicond. Sci. Technol.* **31** 115005
[24] Baboli M A, Slocum M A, Kum H, Wilhelm T S, Polly S J, Hubbard S M and Mohseni P K 2019 *CrystEngComm* **21** 602
[25] Zhuang Q D, Anyebe E A, Sanchez A M, Rajpalke M K, Veal T D, Zhukov A, Robinson B J, Anderson F, Kolosov O and Fal'ko V 2014 *Nanoscale Res. Lett.* **9** 321
[26] Anyebe E A, Sandall I, Jin Z, Sanchez A M, Rajpalke M K, Veal T D, Cao Y, Li H, Harvey R and Zhuang Q 2017 *Sci. Rep.* **7** 46110
[27] Hong Y J, Lee W H, Wu Y, Ruoff R S and Fukui T 2012 *Nano Lett.* **12** 1431
[28] Wang G, Zhang M, Zhu Y, Ding G, Jiang D, Guo Q, Liu S, Xie X, Chu P K and Di Z 2013 *Sci. Rep.* **3** 2465
[29] Dai J, Wang D, Zhang M, Niu T, Li A, Ye M, Qiao S, Ding G, Xie X and Wang Y 2016 *Nano Lett.* **16** 3160
[30] Johansson J, Karlsson L S, Patrik T. Svensson C, Mårtensson T, Wacaser B A, Deppert K, Samuelson L and Seifert W 2006 *Nat. Mater.* **5** 574